Available online at www.sciencedirect.com
SCIENCE DIRECT®
Journal of Sound and Vibration 286 (2005) 21–36
JOURNAL OF SOUND AND VIBRATION
www.elsevier.com/locate/jsvi

Measurements of the acoustic attenuation by single layer acoustic liners constructed with simulated porous honeycomb cores

N. Hillereau, A.A. Syed, E.J. Gutmark*

Gas Dynamics and Propulsion Laboratory, Department of Aerospace Engineering and Engineering Mechanics, University of Cincinnati, Cincinnati, OH 45221-0070 00610, USA

Received 7 August 2003; received in revised form 20 September 2004; accepted 24 September 2004
Available online 24 December 2004

Abstract

An experimental investigation into the acoustic suppression by single layer liners with simulated porous honeycomb cores was conducted. The porous honeycomb was simulated by means of porous partitions whose resistance was varied between zero (no partitions) and infinity (impervious partitions). In addition to the resistance of the porous partitions, variation in the face sheet resistance was also included in the test matrix. A wave tube test apparatus was designed, fabricated and set up. An array of 16 transducers was used to measure the acoustic field in the wave tube. This allowed measuring of the acoustic attenuation data for the different liner configurations. These data showed that for a given value of the face sheet resistance, the variation in the resistance of the porous honeycomb had a significant impact on the acoustic attenuation.

1. Introduction

Acoustic liners are extensively used in the nacelles of turbofan engines for commercial aircraft. The purpose of these liners is to absorb some of the noise generated by the fan before it radiates out of the fan inlet and the fan exhaust ducts. In some instances, acoustic liners are also used in the exhaust duct of the core engine to attenuate combustion and turbine noise. These acoustic

*Corresponding author. Fax: +1 513 556 5038.
E-mail address: Ephraim.Gutmark@uc.edu (E.J. Gutmark).

0022-460X/$ - see front matter © 2004 Elsevier Ltd. All rights reserved.
doi:10.1016/j.jsv.2004.09.029

Nomenclature

c	speed of sound
f	acoustic frequency
h	the depth of the liner cavity
i	$\sqrt{-1}$
k	acoustic wavenumber, $k = 2\pi f/c$
m	the coefficient of mass reactance
n	a positive integer, including zero
p	acoustic pressure
H	the height of wave tube cross section
L	length of the tube ($L = 0.635$ m)
W	the width of wave tube cross section
x	location from source plane along the length of wave tube
R	normalized acoustic resistance
X	normalized acoustic reactance
Z	normalized acoustic impedance; $Z = R + \mathrm{i}X$
sdof	single-degree-of-freedom (single layer) acoustic liner
A_N	complex coefficient of the forward propagating mode in segment #N
B_N	complex coefficient of the backward propagating mode in segment #N
β	the blockage (fraction of 1) of the porous sheet used for partitions
$C_{N,1}$	the complex ratio $\overline{s_N(f)s_1^*(f)}/\overline{s_1(f)s_1^*(f)}$, the calibration of transducer #N relative to transducer #1. $s_1(f)$ and $s_N(f)$ are the signals sensed by the transducers when subjected to identical pressure oscillation $p(f)$
$H_{N,1}$	the complex ratio, $\overline{p_N(f)p_1^*(f)}/\overline{p_1(f)p_1^*(f)}$, of the acoustic pressures measured by the transducer #N and the reference transducer #1. The over-bars denote the time averaging process in signal analysis

liners, based on the Helmholtz resonator principle, are normally of single or double layer design. A great deal of attention is paid to the design and the fabrication of these liners to maximize their effectiveness in order to meet the international noise regulations and the noise requirements of some airports.

Conventional single-degree-of-freedom (sdof) or "single-layer" acoustic liners are constructed with honeycomb core that has impervious cell walls. This ensures that there is little acoustic transmission across the walls of honeycomb cells. It allows the liner to be treated as a uniform array of Helmholtz resonators. Such liners are called "locally reacting". The acoustic damping occurs due to viscous and rotational losses, as air particles oscillate through the porous face sheet.

The use of a porous honeycomb core will allow sound propagation across the cell walls. Thus some damping of acoustic waves will also occur in the cell walls. Such liners are of the so-called "extended reaction" type. It was postulated [1,2] by some researchers that such liners may perform like bulk absorbers to provide superior attenuation over a wider frequency range than conventional single layer liners. The experiments described in this paper were designed to investigate the impact of porous honeycomb on the acoustic suppression obtained with single layer liners.

Due to the great difficulty and the high cost of fabricating honeycomb cores with porous walls of different porosity, it was decided to simulate the honeycomb core by means of partitions, as illustrated in Figs. 1 and 3. These partitions divide the space behind the face sheet into small cavities in the longitudinal direction. Within the frequency range of interest, the acoustic pressure over the liner has no transverse variation. Therefore, there is no need to subdivide these cavities in the transverse direction to simulate the honeycomb. It was observed [3] that liners with impervious

Fig. 1. Picture of a liner without the face sheet.

partitions, as described above, were "locally reacting" within the frequency range of interest, as defined in this paper. Though not perfect, this simulation is considered to be a very good approximation of honeycomb. Therefore, porous partitions do also simulate porous honeycomb in the direction of sound propagation in the test apparatus.

Earlier experiments [3], conducted at GE Aircraft Engines, showed that compared to the liner with impervious partitions, porous partitions did provide a broader bandwidth of suppression but it was at the cost of reduced suppression near the peak attenuation frequency. In these experiments the honeycomb core was simulated by partitions made of laser-drilled, porous sheet material. The cell size was represented by the spacing between adjacent partitions. The cell depth and the cell wall impedance characteristics were kept unchanged while the cell size was varied. For porous partitions, the best results were obtained with the spacing of 0.00635 m between adjacent partitions.

This earlier work was considered to be preliminary. The work presented in this paper was undertaken to conduct a more systematic and thorough investigation of the acoustic attenuation performance of single layer liners with porous honeycomb cores.

The measurement technique described in this paper, based on the cross-correlation of signals, has been widely used by numerous researchers [5–8], and therefore it is well understood. The success of the technique depends on the care taken in the calibration of the transducer channels used in data acquisition, as highlighted in Section 4.

2. The test apparatus

2.1. Hardware

2.1.1. Liners

The parameters of interest in the design of a liner with porous honeycomb core are as follows: (1) The impedance characteristics of the face sheet which depend on its geometrical details

(thickness, hole-diameter, porosity, etc.). (2) The impedance characteristics of the porous walls of the cells. These depend on its geometric details (effective porosity, hole-diameter of perforations, thickness of cell walls). (3) The depth, h, of the honeycomb core and (4) the size of the cell.

The experiments were designed with constant values of the cavity depth ($h = 0.0254$ m), and the size of the honeycomb cell (0.00635 m). The honeycomb was simulated by means of partitions at a spacing of 0.00635 m. A liner sample, without the face sheet, is shown in Fig. 1.

It was decided to use so-called "linear" materials as face sheets in order to avoid additional complexity due to the sensitivity of the acoustic impedance to the acoustic excitation levels. Three wire-mesh-on-perforate type sheets were selected to simulate the variation in the impedance parameters of the face sheet.

A laser drilled fiberglass-epoxy sheet simulated the porous honeycomb. The variation in the resistance and the mass reactance of the porous partitions was achieved by the blockage of a fraction of the holes in the sheet. This concept is illustrated in Fig. 2. Two different orientations of the blockage strips were used, normal and parallel to the face sheet. The nominal values of blockage used for the acoustic liner samples are shown in Table 1. The blockage value of 100% signifies impervious partitions. The value of 0% blockage refers to the baseline (laser drilled) porous sheet material. An additional liner with no partition in the cavity was also included for testing. Parameters for the porous sheet partitions in the acoustic liner test samples are shown in Table 2.

The case of no partitions represents zero impedance—the opposite of zero admittance, for the impervious partitions. Thus a wide variation in the impedance of porous partitions was simulated in the nine different cavities described above. Each one of these liner cavities was tested with three different face sheets. Thus 27 different single layer liners were tested (Table 3).

2.1.2. The wave tube

The acoustic measurements were conducted in the wave tube shown in Figs. 3 and 4. The wave tube was of 0.0381-m $\times$0.0381-m cross section and 0.635 m long. On one end it was attached to an acoustic driver and on the other end an acoustically absorptive termination was provided by a 0.0762 m deep cavity filled with "bulk absorber" foam material. The acoustic liner was installed in the middle of the wave tube, as shown in Fig. 3, to measure its acoustic attenuation.

A total of 16 miniature piezoresistive pressure transducers, (Endevco model 8506-2) were installed to measure the acoustic field in the wave tube. There were two objectives for the acoustic measurements. These were: (1) to measure the acoustic attenuation obtained by the liner sample

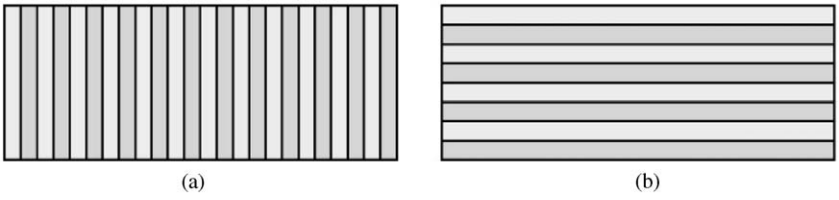

Fig. 2. Diagram showing stripes of blockage which increase the resistance and the mass reactance of the porous sheet used for partitions: (a) 6 samples; (b) 2 samples.

Table 1
Nominal values of blockage

Sample no.	1	2	3	4	5	6	7[a]	8[a]
Blockage (%)	0	40	60	70	80	100	60	80

[a]The samples 7 and 8 were with the strips of blockage parallel to the face sheet.

Table 2
Parameters for the porous sheet partitions in the acoustic liner test samples: the effective porosity (POA), the normalized resistance (R) and the mass reactance coefficient (m) for different values of the blockage

Sample no.	Blockage (%)	Effective POA	Coeff of mass reactance m (m)	Specific acoustic resistance R
1	0	6.7	0.0071	0.57
2	40	4	0.0119	0.94
3	60	2.7	0.0178	1.41
4	70	2	0.0236	1.88
5	80	1.3	0.0356	2.83

Table 3
Acoustic resistance and the coefficient of mass reactance data for the three face sheets

Face sheet number	Resistance R	Mass reactance coefficient (m)
1	0.14	0.0074
2	1.25	0.0056
3	1.68	0.0045

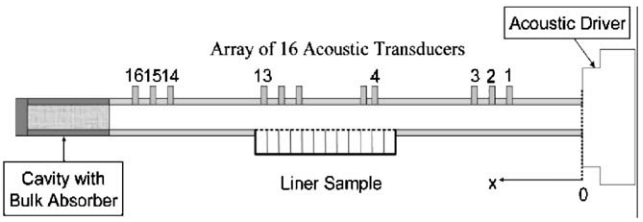

Fig. 3. Schematic diagram of the acoustic wave tube apparatus with the acoustic liner.

with the transducer arrays (1, 2, 3) and (14, 15, 16); and (2) to educe the acoustic characteristics of the liner sample from the data measured just over it by the transducers #4 through #13.

The work of analyzing the data from transducers #4 through #13 is in progress at NASA Langley Research Center. The results of this analysis, when completed, will be published in a separate paper.

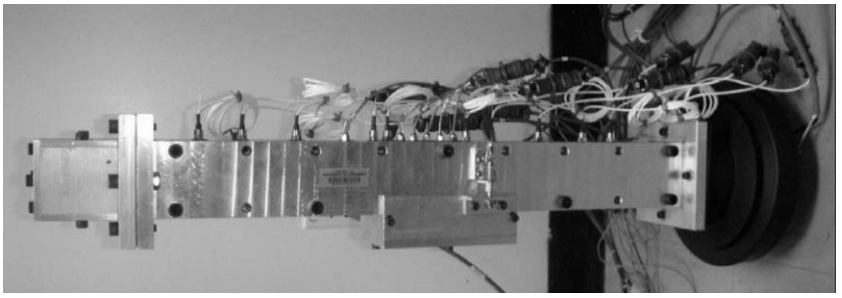

Fig. 4. Photograph of the acoustic wave tube.

2.2. Software

LabVIEW programming was developed for the acquisitions and the processing of the transducer signals and for the computation of the acoustic attenuation spectra from the measured data. The theory behind the calculation is described below.

3. Theoretical background

3.1. Wave propagation in the hard wall segments

Sound propagation in a hard-walled rectangular duct of uniform cross section, as illustrated in Fig. 3, can be expressed in terms of the solutions (modes) of the wave equation, as

$$p(x,y,z,t) = \sum_m \sum_n (A_{mn}\exp\{-\mathrm{i}k_{mn}x\} + B_{mn}\exp\{\mathrm{i}k_{mn}x\})\cos\left(\frac{m\pi y}{H}\right)\cos\left(\frac{n\pi z}{W}\right)\exp(\mathrm{i}\omega t), \quad (1)$$

where $m = 0, 1, 2, 3, 4, \ldots$, $n = 0, 1, 2, 3, 4, \ldots$, p is the acoustic pressure, A_{mn} and B_{mn} are the coefficients of the forward and backward propagating modes, $\omega = 2\pi f$ is the angular frequency, f is the acoustic driving frequency, H is the duct height, W is the width of the duct, and k_{mn} is the axial wavenumber defined by the dispersion relationship

$$k_{mn} = \sqrt{\{k^2 - \eta_{mn}^2\}}, \quad (2)$$

where $k = \omega/c = 2\pi f/c$, $\eta_{mn}^2 = (m\pi/H)^2 + (n\pi/W)^2$.

It can be shown that for an acoustic mode to propagate and transmit acoustic energy, k_{mn} must be real [4]. This condition is satisfied if

$$k \geqslant \eta_{mn}. \quad (3)$$

Eq. (3) defines the frequencies at which an acoustic mode, of order (m,n), is able to propagate and transmit acoustic energy. The mode "cut-on frequency" is defined as

$$(f_{mn})_{\text{cut-on}} \geqslant \frac{c}{2\pi}\eta_{mn}. \quad (4)$$

For frequencies at or above the cut-on frequency, the (m,n) mode can propagate. At frequencies below the cut-on frequency the (m,n) mode is naturally damped and cannot propagate. Note that the plane wave mode (0,0) can propagate at all frequencies.

In this research project, measurements were limited to frequencies below the cut-on frequency of the first transverse mode ($m=1, n=0$). For the duct height of 0.0381 m, the cut-on frequency of the first transverse mode, at room temperature (294 K), is 4500 Hz approximately. Therefore, the acoustic wave propagation is reduced to a one-dimensional problem, as schematically illustrated in Fig. 6. Below the cut-on frequency of the first transverse mode (4500 Hz), the acoustic pressure at any location x, is given by

$$p(x,f) = A\ \exp(-\mathrm{i}kx) + B\ \exp(\mathrm{i}kx). \tag{5}$$

The transfer function for the acoustic pressures measured by a transducer #N, and the reference transducer #1, is defined as

$$H_{N,1}(f) = |H_{N,1}(f)|\exp(\mathrm{i}\phi_{N,1}) = \frac{\overline{p_N(f)p_1^*(f)}}{\overline{p_1(f)p_1^*(f)}}, \tag{6}$$

where $N = 2$ to 16. The over-bars in Eq. (6) denote the time-averaging process.

3.2. Relative calibration

The calibration of each transducer (#N), relative to the reference transducer (#1), was conducted in a tube of 0.03175 m diameter. The transducers were flush mounted in a hard wall termination at one end of the tube while the other end was connected to a sound source. Up to the frequency for the cut-on of the first circumferential mode, the two transducers were subjected to identical acoustic signals. The relative calibration of the two transducers (the reference transducer #1 and transducer N) is defined as

$$C_{N,1}(f) = \frac{\overline{s_N(f)s_1^*(f)}}{\overline{s_1(f)s_1^*(f)}}, \tag{7}$$

where $N = 2$ to 16; $s_1(f)$ and $s_N(f)$ are the voltage signals from the transducers when subjected to identical pressure oscillation $p(f)$.

The measured values of the complex transfer-function $H_{N,1}(f)$, as defined in Eq. (6) are corrected as

$$H_{N,1}(f)_{\text{corrected}} = \frac{\{H_{N,1}(f)\}_{\text{measured}}}{\{C_{N,1}(f)\}_{\text{calibration}}}. \tag{8}$$

3.3. Verification of the relative calibration

After the calibration process was completed, the transducers were installed in the tube at locations $x_1, x_2, x_3, \ldots, x_N$; as illustrated in Fig. 5. The walls of the wave tube were acoustically hard throughout its length. In addition, there was a hard wall termination at $x = 0.635$ m. The verification of calibration consisted of a comparison of the measured data with the theoretical

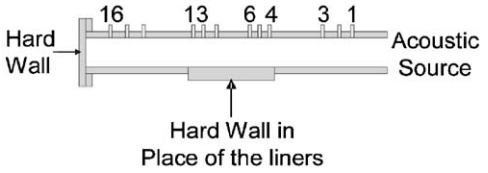

Fig. 5. Schematic diagram of the wave tube with two acoustically hard walls: one in place of the acoustic liner and a hard-wall termination at $x = 0.635\,\mathrm{m}$.

values given by

$$\{H_{N,1}(f)\}_{\text{corrected}} = A_{N,1}(f)\mathrm{e}^{\mathrm{i}\phi_{N,1}} = \frac{\cos\{k(x_N - L)\}}{\cos\{k(x_1 - L)\}}, \tag{9}$$

where L is the length of the wave tube ($L = 0.635\,\mathrm{m}$).

3.4. Acoustic attenuation

In the configuration illustrated in Fig. 6, the wave tube is divided into three segments. In segments 1 and 3, both opposite walls are acoustically hard. In segment 2, one of the walls is lined with an acoustically absorptive liner. The acoustic field in segment #1 consists of forward ($+$ x-direction), and backward propagating plane waves. From the acoustic data, measured at locations 1, 2, and 3, the following set of linear equations can be obtained:

$$\begin{bmatrix} \exp(-\mathrm{i}kx_1) & \exp(\mathrm{i}kx_1) \\ \exp(-\mathrm{i}kx_2) & \exp(\mathrm{i}kx_2) \\ \exp(-\mathrm{i}kx_3) & \exp(\mathrm{i}kx_3) \end{bmatrix} \quad \begin{Bmatrix} A_1 \\ B_1 \end{Bmatrix} = \begin{Bmatrix} 1 \\ \tilde{H}_{2,1} \\ \tilde{H}_{3,1} \end{Bmatrix} p_1(x,f). \tag{10}$$

Similarly, from the data measured at locations 14, 15, and 16, we get the following set of linear equations:

$$\begin{bmatrix} \exp(-\mathrm{i}kx_{14}) & \exp(\mathrm{i}kx_{14}) \\ \exp(-\mathrm{i}kx_{15}) & \exp(\mathrm{i}kx_{15}) \\ \exp(-\mathrm{i}kx_{16}) & \exp(\mathrm{i}kx_{16}) \end{bmatrix} \quad \begin{Bmatrix} A_3 \\ B_3 \end{Bmatrix} = \begin{Bmatrix} \tilde{H}_{14,1} \\ \tilde{H}_{15,1} \\ \tilde{H}_{16,1} \end{Bmatrix} p_1(x,f). \tag{11}$$

Eqs. (10) and (11) can be solved to obtain the complex coefficients A_1, B_1, A_3, B_3. The acoustic attenuation (dB) due to the liner is defined as

$$\text{Attenuation (dB)} = 10\,\mathrm{Log}_{10}\frac{|A_1|^2}{|A_3|^2}. \tag{12}$$

Note that the reflected or backward propagating coefficients are not included in the calculation of the acoustic attenuation.

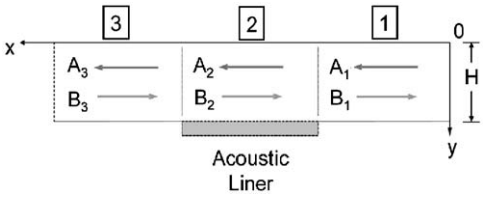

Fig. 6. Schematic diagram of acoustic wave propagation in a two-dimensional duct.

4. Results and discussion

In each of the two hard wall segments, we needed to determine two unknown coefficients (A and B) for which we required only two equations, and therefore, acoustic measurements at only two locations. Instead we measured data at three locations. Thus the values of the coefficients determined from Eqs. (10) and (11) represent a least-squares fit of the measured data at three locations. It also provides accurate data over a larger range of frequencies than obtained with measurements at only two locations. The spacing between the transducers was determined to provide good accuracy between 500 and 4000 Hz.

The acoustic test data have to be accurate, repeatable, and reproducible so that any conclusions from these data may be drawn with confidence. Therefore, a test process and procedures, described in Fig. 7, were established to accomplish this. The experiments were conducted in four steps: (1) a relative calibration of the transducers was performed to correct for any differences of sensitivity or phase when the transducers were subjected to an identical acoustic signal; (2) a verification of this calibration, devised to conduct an in situ check of the relative calibration of all transducers; (3) the attenuation tests of the liner test samples; and (4) attenuation tests with a different orientation of the blockage strips to check if this orientation has an impact on the acoustic attenuation.

4.1. Relative calibration of the acoustic transducers

The rationale for the relative calibrations is to correct for the small differences in the response characteristics of the different transducers to identical acoustic signals. An example of the calibration of transducer #2 relative to the reference transducer #1 is shown in Figs. 8 and 9.

If transducers #1 and #2 had identical response characteristics, then the calibration, $C_{2,1}(f)$, would be unity at all frequencies. However, real transducers have slightly different response due to variations in manufacturing processes. In addition, the signal conditioning amplifiers and cables also contribute to differences in response. Therefore the real part of the calibration $C_{2,1}(f)$ is expected to be close to unity, and the imaginary part is expected to be close to zero. This is what is shown in Figs. 8 and 9. Note that the measured calibration data show slight sinusoidal contamination, which seems to grow in magnitude with increasing frequency. This is probably due to the contribution of the first higher order cut-off mode ($m = 1$) in the calibration fixture. Alternatively, this may be due to resonance phenomena based on the overall length of the tube. The data were smoothed by fitting second-order polynomials through measured values between

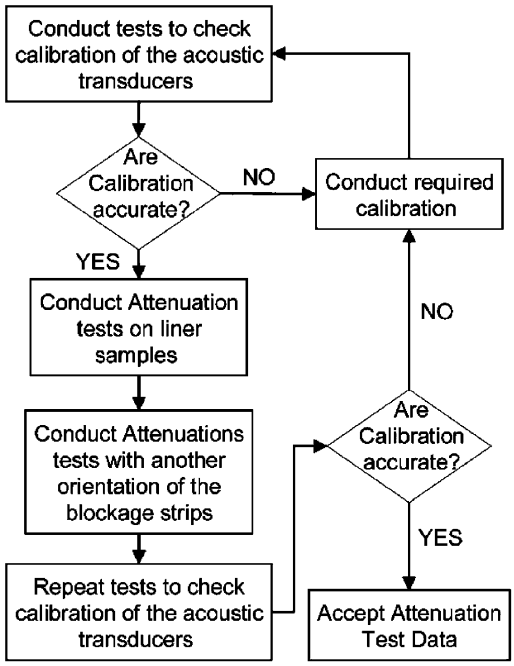

Fig. 7. The process map used for conducting attenuation tests on acoustic liner samples in the wave tube apparatus.

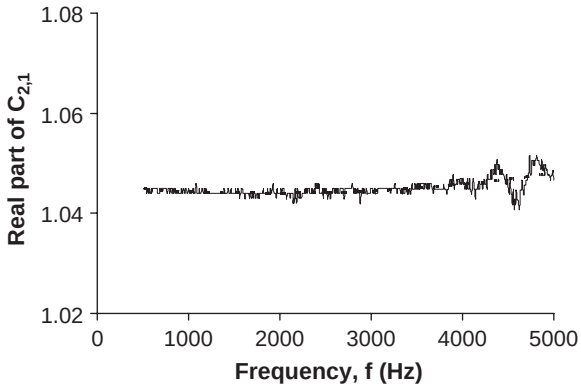

Fig. 8. Plot of the real part of the relative calibration, $C_{2,1}(f)$, against frequency. Polynomial equation: $C_{2,1} = 4.349\text{E-}10f^2 - 1.688\text{E-}6f + 1.046$. Solid line for measured calibration data and dashed line for a polynomial fit.

500 and 5000 Hz. These polynomials were used to generate calibration data files that were used to correct all subsequent test data.

4.2. Calibration checks

The measured data for the transfer-function, $H_{3,1}(f)$, of pressures at locations #3 and #1 are shown in Figs. 10 and 11. The measured values of the magnitude and the phase indicate a small

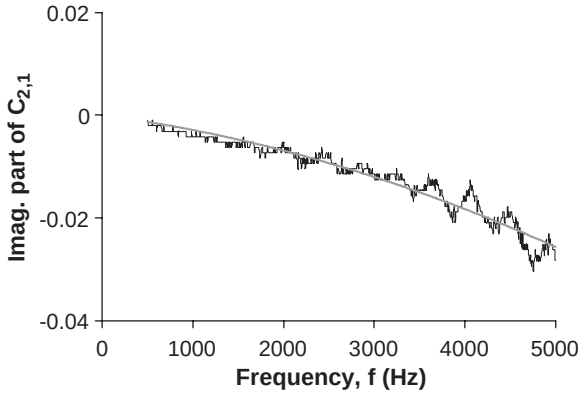

Fig. 9. Plot of the imaginary part of the relative calibration, $C_{2,1}(f)$, against frequency. Polynomial equation: $C_{2,1} = -5.620\text{E-}10f^2 - 2.323\text{E-}6f$. Black thin line for measured calibration data and gray thick line for a polynomial fit.

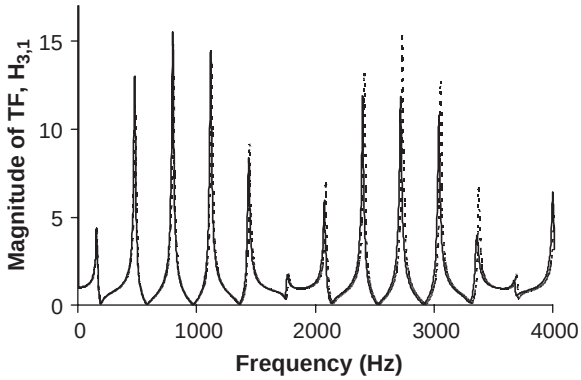

Fig. 10. Comparison of the measured and the computed values of the magnitude of the transfer function $H_{3,1}(f)$. Solid line for measured data and dashed line for computed results.

amount of damping in the wave propagation inside the wave tube. Thus, good agreement between the measured and the computed data was obtained when a damping coefficient value of 0.118/m was used. It is noted that this value for the damping coefficient is a rough approximation only. The test data indicate that the damping varies with frequency.

Examination of Fig. 10 shows that the difference between the computed and the measured data can be significant at the frequencies of the peaks of the transfer-function, $H_{3,1}(f)$. At these frequencies, the acoustic pressure at the reference transducer approaches zero. Therefore, measurement uncertainties are magnified. These frequencies are given by

$$f_n = \frac{(2n+1)c}{4x_1}, \tag{13}$$

where $n = 0, 1, 2, 3, 4, \ldots$.

Another way to check the accuracy of the transducer calibrations is to plot the ratio of the acoustic pressure at any location x (from the hard termination), and the pressure at the reference

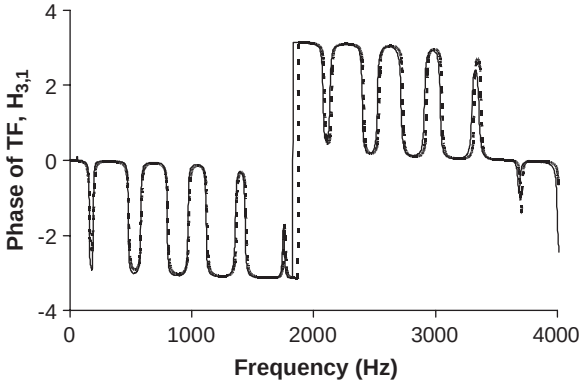

Fig. 11. Comparison of the measured and the computed values of the phase of the transfer function $H_{3,1}(f)$. Solid line for measured data and dashed line for computed results.

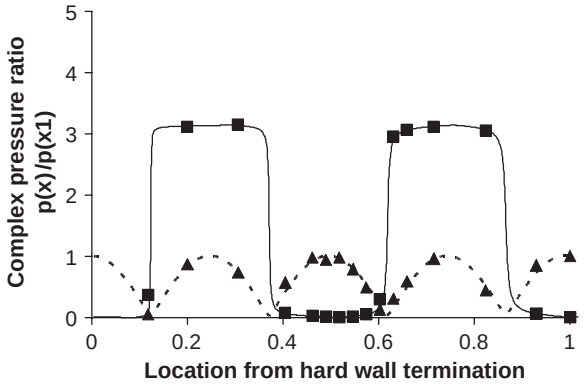

Fig. 12. Comparison of the computed and the measured values of the complex ratio $p(x,f)/p(x_1,f)$. A damping rate of 0.118/m was used in the computed data. Solid line for H phase theory, dashed line for H magnitude theory, squares for H phase measured, and triangles for H magnitude measured.

location #1. A typical example of such plots is shown in Fig. 12. It shows the measured and the computed values of the magnitude and the phase of the ratio $p(x)/p(x_1)$, plotted against the location, x. There is very good correlation between the computed data and the measured values at the 16 transducer locations.

The calibration checks were performed before and after conducting the tests on the acoustic liner configurations of Table 1. The quality of these checks was judged to be satisfactory.

4.3. Acoustic attenuation data

4.3.1. Repeatability of testing

Before any discussion of the trends observed from the measured attenuation data, it is appropriate to discuss the repeatability of the test data. Fig. 13 shows the data from four different tests on the same liner configuration. The three continuous plots represent data

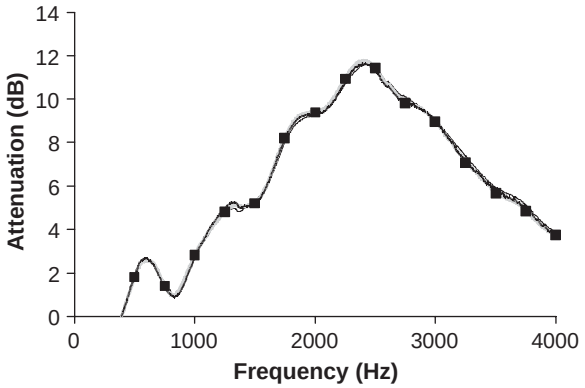

Fig. 13. Plots show typical examples of the repeatability of measured attenuation spectra. Continuous charts were obtained with broadband excitation. The squares show data obtained with discrete excitation. Solid line for first test, dotted line for second test, dashed line for third test, and squares for test with tones.

measured with broadband excitation. The frequency step for these measurements is 4.88 Hz. Thus, between 500 and 4000 Hz, there are over 700 frequency points for which attenuation data is computed. The fourth set of data was obtained with discrete (tonal) excitation. It is clear from Fig. 13 that within the measurement repeatability, the data from the tests with tones are not different from those obtained with broadband excitation. This is what was expected from the so-called linear sheet materials used in the construction of liner test samples.

4.3.2. The effects of the orientation of the blockage strips on the porous partitions

The two liner cavities with partitions that had the blockage stripes parallel to the face sheet were also tested with each of the three face sheets. Fig. 14 shows that the orientation of the blockage stripes had little impact on the attenuation spectra. Any observable differences may be due to small differences in blockage and due to measurement repeatability.

4.3.3. The effects of changing the impedance of the porous partitions

The impedance of the porous partition was varied from 0 (no partitions) to very large values (impervious partitions). The effects of this variation on the attenuation are plotted for each of the three face sheets in Figs. 15–17.

It can be seen that for each face sheet, the effect of reducing the impedance of partitions caused some improvement in the attenuation at higher frequencies. However, this was achieved at the expense of reduction in suppression near the frequency of peak attenuation.

4.3.4. The effects of changing the impedance of the face sheet

It can be observed from the plots in Fig. 18 that the impedance characteristics of the face sheets have a strong impact on the attenuation achieved by a liner.

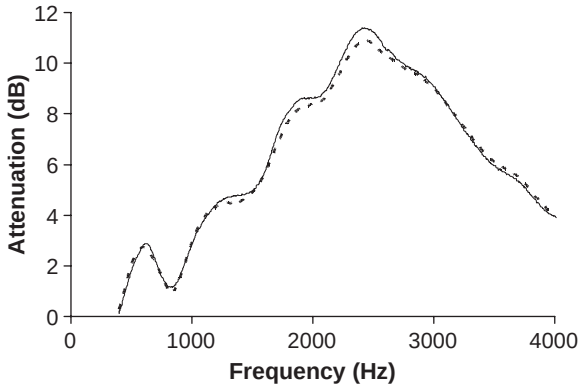

Fig. 14. Plots of attenuation spectra show the effect of changing the orientation of the blockage strips. Dashed line for horizontal strips and solid line for vertical strips.

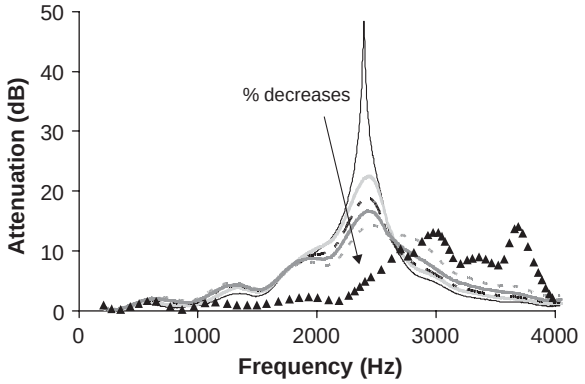

Fig. 15. Plots of attenuation spectra show the effects of changing the impedance of the porous partitions. These data were measured with the face sheet #1: —, 100%; ——, 80%; — —, 60%; ——, 40%; - - - -, 0%; ▲, no partition.

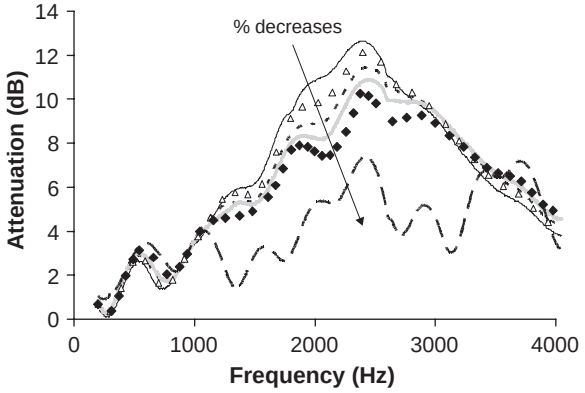

Fig. 16. Plots of attenuation spectra show the effects of changing the acoustic impedance of the porous partitions. These data were measured with the face sheet #2: —, 100%; △, 80%; - - - -, 60%; ——, 40%; ◆, 0%; — —, no partition.

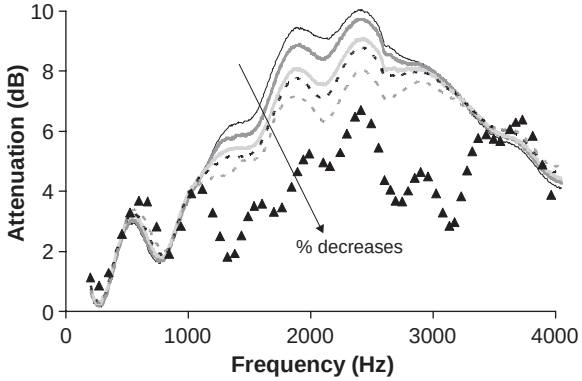

Fig. 17. Plots of attenuation spectra show the effects of changing the acoustic impedance of the porous partitions. These data were measured with the face sheet #3: —, 100%; ——, 80%; ——, 60%; - - - -, 40%; - - - -, 0%; ▲, no partition.

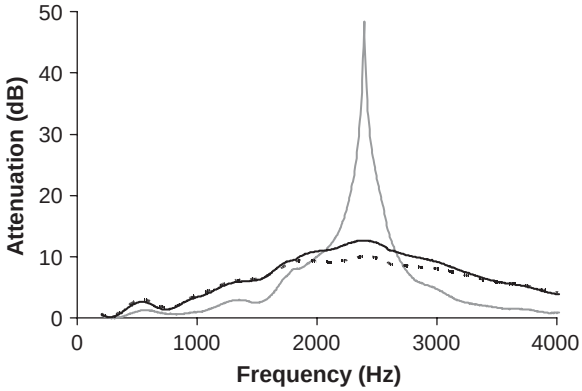

Fig. 18. Plots show the effects of changing the impedance of the face sheet on the attenuation spectra. Face sheet #1 has the highest and face sheet #3 has the lowest value of acoustic resistance. These data were measured with impervious partitions: ——, sheet 1; — —, sheet 2; - - - -, sheet 3.

5. Conclusions

The simulation of porous honeycomb by means of porous partitions is considered to be satisfactory for the experiments with single mode propagation, described in this paper. It is not a complete simulation of the multi-mode propagation over an acoustic liner in an engine duct. However, the data presented in this paper may point to a possible impact on the attenuation performance of a honeycomb with porous cell walls, if incorporated in liner design. An examination of the test data leads to the following conclusions:

- The robust test apparatus and measurement technique described in this paper are capable of accurate and repeatable measurements of (1) the normal acoustic impedance; and (2) the (single mode) acoustic attenuation (dB) for acoustic liner samples.

- A reduction in the resistance of the porous partitions results in reduced suppression at and near the peak of the attenuation spectrum, and a small increase in suppression at higher frequencies. The reduction in suppression at and below the peak frequency is much larger than the corresponding increase in suppression at the higher frequencies.
- For given values of the cavity depth and the face sheet resistance, the best attenuation results appear to be achieved by impervious partitions. Thus, locally reacting liners represent the most effective acoustic design.
- Fluid drainage slots, incorporated in the honeycomb core of single or double layer acoustic liners installed in aircraft engine ducts, can significantly impair their sound suppression capability.

Further investigation into the impact of drainage slots will continue.

Acknowledgements

The authors wish to recognize the help and contribution of S. Baujard and R. DiMicco in the completion of this NASA sponsored research project.

References

[1] United States Patent No. US 6,182,787 B1, February 2001, Inventors: Robert E. Kraft, Asif A. Syed.
[2] G. Bielak, et al., Advanced Nacelle Acoustic Lining Concepts Development, NASA CR-2002-211672, August 2002.
[3] R.E. Kraft, Contribution to the final report prepared by GE Aircraft Engines on NASA Contract NAS3-98004, Task Order 13.
[4] W. Eversman, Energy flow criteria for acoustic propagation in ducts, *Journal of the Acoustical Society of America* (1970).
[5] A.A. Syed, D.L. Lewis, The measurement of acoustic suppressions in a flow duct using an energy flux measurement technique, in: *AIAA 13 Aeroacoustics Conference*, October 1990, Paper Number AIAA-90-3949.
[6] M. Salikuddin, A.A. Syed, P. Mungur, Acoustic characteristics of perforated sheets with through-flow in high intensity noise environment, in: *AIAA 13 Aeroacoustics Conference*, October 1990, Paper Number AIAA-90-3931.
[7] J.W. Kooi, S.L. Sarin, An experimental study of the acoustic impedance of Helmholtz resonator arrays under a turbulent boundary layer, AIAA Paper No. 81-1998, 1981.
[8] P.D. Dean, An in-situ method of wall acoustic impedance measurement in flow ducts, *Journal of Sound and Vibration* 34 (1) (1974) 97–130.